Received: 10 September 2023 | Revised: 11 October 2023 | Accepted: 23 October 2023

IET Electric Power Applications

DOI: 10.1049/elp2.12384

The Institution of Engineering and Technology WILEY

ORIGINAL RESEARCH

Incorporating the coupled effects of slot opening, armature reaction and saturation in the model of the airgap flux density distribution of permanent magnet synchronous machines

Mojtaba Babaei[1] | **Mojtaba Feyzi**[2] | **Abbas Nazari Marashi**[2]

[1]Department of Electrical and Computer Engineering, Yadegar-e-Imam Khomeini (RAH), Shahr-e-Rey Branch, Islamic Azad University, Tehran, Iran

[2]Electrical Machines Research Group, Khaje Nasir University of Technology Branch, ACECR, Tehran, Iran

Correspondence

Mojtaba Babaei.
Email: mba_babaei@yahoo.com; mojtaba_babaei@iausr.ac.ir

Abstract

A new analytic model for calculating of the air-gap flux density (AGFD) of surface-mounted permanent magnet synchronous machines (SMPMSMs) is presented. This proposed model is capable to taking into account the effects of magnetic saturation, armature reaction and stator slots opening. Furthermore, the real form of air-gap distribution and spatial distribution of flux density of the PM poles are considered. The armature reaction effect is modeled using phasor diagram analysis of the motor as a function of the load torque, the armature current amplitude, power factor and the inverse air gap length. Also, saturation phenomenon predicted using the new non-linear proposed function in connection with the armature reaction effects and the properties of the lamination material. It is shown that the proposed model capable to predicting acceptably the air gap flux density waveform of the SMPMSMs at lagging and leading power factors and with the load torque variation. The presented analytical approach is verified by the two-dimensional finite-element analysis (FEA) results.

KEYWORDS

finite element analysis, fourier series, magnetic flux, permanent magnet machines

1 | INTRODUCTION

Permanent magnet synchronous motors (PMSMs) are a suitable option for using at industrial and control applications due to their high efficiency, high power density, suitable dynamic behaviour and good controllability. The accurate prediction of the dynamic behaviour in different conditions as well as the appropriate design of the control systems of the motor require the availability of a comprehensive and correct dynamic model. The key to the dynamic modeling of the PMSMs is the calculation of the flux linkage of the winding and the permanent magnet poles, and this parameter, in turn, depends on the air gap flux density [1]. The accurate calculation of the flux density distribution in the air gap of the PMSMs also makes it possible to predict important characteristics of the motor, such as cogging torque, back electromotive force (back-EMF), torque ripple and unbalanced magnetic pull (UMP), along with the exact harmonic analysis of the motor in healthy and faulty conditions [2–4]. Furthermore, this accurate prediction can be used in design optimization at the early stages of PMSMs design procedure [[5–7].

The main influencing factors in the distribution form of the air gap flux density in PMSMs with specific geometric dimensions are (1) shape and number of the slots and the permanent magnets, (2) the coils distributed in the stator slots, (3) amplitude of the stator current, (4) the position of the rotor, (5) the magnetic saturation, (6) degree of the armature reaction, (7) the power factor and (8) the torque of mechanical load. Some of these factors act as a couple and affect each other. Incorporating the effects of these factors into the air gap flux density model of the PMSMs can lead to achieving a precise and comprehensive dynamic model of the motor at different operation conditions. The main goal of this article is to present such model with its numbered characteristics. Of course, these

works should be considered with simplicity and precision in order to avoid complications.

So far, many works have been conducted in the field of prediction and modeling of air gap flux density waveform in PMSMs. The general characteristic of these models is a compromise between accuracy, speed and cost, which off course corresponds to reality. It seems that none of these works have included the feature of comprehensiveness in the model. In [8–11], the magnetic field in surface-mount and interior PMSMs is calculated in the no-load condition and the main emphasis is on the effect of the shape of the PM poles. An analytical model of the healthy and eccentric PMSMs is presented using two types of conformal mappings at no-load condition in [12, 13], respectively. Also, using the magnetic equivalent circuit (MEC), non-linear magnetic analysis of a large turbo-generator is presented under the no-load condition [14]. Using the 3D sub-domain analytical approach, magnetic flux density in induction machines with semi-closed slots is calculated under the no-load condition [15]. The air gap magnetic flux density and cogging torque for several different PM ploes cutting sizes at the no-load condition are obtained with the method of separating variables [16]. Related papers such as [17–21] predicted air gap field distribution in PMSMs in the open-circuit condition. These references are used well-known analytical methods such as MEC [17], improved permeance model [18], lumped magnetic parametric model [19], subdomain model [20], and piecewise inverse cosine function (PICF) [21]. By reviewing the models and works presented in these valuable nine references, it can be concluded that the models are accurate and practical in no-load or open-circuit conditions. While it is obvious at PMSMs under load conditions, many factors, such as the armature current, the magnetic saturation, the armature reaction, the power factor and the load torque, can be the effective and must be considered in the models. Based on this fact, number of references have considered the mentioned effects of on-loading of the PMSMs in the analytical model of the magnetic field. In [22], by combining conformal mapping and MEC method, the saturation effect is incorporated into the model of a surface PMSMs at on-load condition. In [23], an equivalent air gap function is proposed that is capable of taking into account the saturation and armature reaction of an interior PMSM. Magnetic field of a saturated eccentric PMSM is predicted using combined magnetic circuit and subdomain method [24]. Also, the influencing of the shape, dimension and direction of magnetization of the PM poles in the field distribution waveform of the air gap of the permanent magnet motors are investigated [25–27]. Using the modified phase field model, the method proposed in ref. [25] has been able to reduce air gap field harmonics by proposing different forms of permanent magnet poles. A 2D analytical model is presented in [26] for consequent-pole slotted stator PMSMs to calculate the magnetic field distribution due to PMs and armature reaction. Optimal PM-Arc ratio of consequent poles is proposed in [27] to improve the utilisation of PM material and increase the output torque. Using the subdomain technique, the slotting and tooth-tip effects are also taken into account [28]. Skewed slots effects on air gap flux density distribution of a surface-mounted PM machine are also investigated using 3D analytical model-based Maxwell's equations [29].

By studying the above-mentioned references, it can be concluded that the comprehensive model of the AGFD in PMSMs with specific ability is not addressed in the existing literatures. We attempt to create a detailed analytic model for AGFD distribution of the SMPMSMs to cover the mentioned important factors. Therefore, in the present paper:

(1) Using phasor diagram analysis, the effect of armature reaction will be modeled as a function of different variables, such as the load torque, the power factor and the armature current amplitude.
(2) A new model of saturation phenomenon in connection with the armature reaction effects is introduced that is capable of taking into account the effects of load torque and power factor variation on the saturation degree.
(3) Fourier series of the extended inverse air gap function of the SMPMSM including the slotting effect is presented.
(4) A new form of the Magneto-motive force (MMF) of the stator winding and Fourier series of the MMF distribution of the PM poles are proposed, which can consider both AR and saturation phenomenon interdependently.
(5) The sensitivity analysis of the proposed analytical model is presented at different operating conditions.
(6) The ability of the proposed comprehensive model results is verified by FE results.

2 | APPROACH FOR CALCULATION OF AGFD OF THE SMPMSM

For the PMSM machine, the MMF of the air gap consists of two components: MMF of the stator (armature) and MMF of the rotor (PM poles). When the spatial distribution of the armature winding is known, the rotating MMF produced by the applied current can be described using the Fourier series function. The MMF distribution for various winding types including concentrated winding and distributed winding topology has been widely studied in many literatures [30–33] as a general expression. Such the general function is modeled through the following equation:

$$\mathrm{MMF}_s(\varphi_s, \theta_r) = \sum_{n=1} \frac{3}{2} \frac{2}{\pi} \frac{N_s K_w}{n} I_a \cos(\theta_r - nP\varphi_s - \varnothing_i) \quad (1)$$

where the φ_s, θ_r and $\varnothing_i$ are the position measured from the stator, rotor position and phase angle at time zero, respectively. Also, N_s, K_w and I_a represent the number of equivalent turns, the winding factor and current amplitude of the stator phases winding, respectively. The mmf distribution of the PM poles established at the air gap can be modeled as follows [30]:

$$\mathrm{MMF}_{\mathrm{pm}}(\varphi_r)=\begin{cases}-\dfrac{d_m B_m}{\mu_0(1+\chi)}, & \alpha_0+\alpha_{\mathrm{pm}}\geq\varphi_{\mathrm{r}}>\alpha_0\\ 0, & \alpha_0+\pi\geq\varphi_{\mathrm{r}}>\alpha_0+\alpha_{\mathrm{pm}}\\ \dfrac{d_m B_m}{\mu_0(1+\chi)}, & \alpha_0+\alpha_{\mathrm{pm}}+\pi\geq\varphi_{\mathrm{r}}>\pi+\alpha_0\end{cases} \tag{2}$$

where the d_m, α_{pm} and B_m are the PM depth, the angular span of the one PM pole and the maximum flux density above the PM poles, respectively. Also, μ_0, α_0 and χ are the vacuum magnetic permeability, the position of the PM pole at time zero and the susceptibility of the PM material, respectively. Also, the position measured from the rotor (φ_r) can be written as follows:

$$\varphi_r=\varphi_s+\theta_r \tag{3}$$

Equation (2) is also be described using the Fourier series function. The value of the B_m is dependent to such variables, including air gap length, PM depth and residual flux of the PM pole, according to the following:

$$B_m=\frac{B_r}{1+\frac{g_{\min}}{d_m}} \tag{4}$$

The resultant air gap flux density of a PMSM can be expressed using substantial relation as follows:

$$B(\varphi_s,\theta_r)=\mu_0\frac{\mathrm{MMF}_s(\varphi_s,\theta_r)+\mathrm{MMF}_{\mathrm{pm}}(\varphi_r)}{g(\varphi_r)} \tag{5}$$

where the g (φ_r) is the air gap function distribution. In a SMPMSM, the air gap is uniform and this function can be considered as a constant value.

A typical SMPMSM with specification given in Table 1 and PM type (NdFeB 42) are considered to simulate the MMF distribution of stator and rotor. Also, the steel-1008 lamination material is applied to the stator and rotor core for precise simulation of the resultant air gap flux density distribution. The magnetization characteristic of the steel-1008 is shown in Figure 1. In addition, Figure 1 represents the MMF distribution of the stator and rotor based on the actual distribution of the 3-phase winding conductors inside the 18-slots of the stator and the two-PM poles. For 3-phases, 2-poles and 18-slots SMPMSM, the machine will have more than 3 slots/poles/phases. In these machines, the steps in the MMF wave are neglected and variation is taken as smooth over these slots. Therefore, the stepped MMF wave changed to a trapezoidal MMF wave calculated using the harmonics components of Equation (1).

TABLE 1 Main geometry data of the surface-mounted PMSM used in the simulation.

Variables	Definition	Values
g_0	Air gap length	3.37, mm
d_m	Permanent magnet depth	1.7, mm
α_{pm}	Angular fraction of a PM pole	0.66
Q_s	Number of slots	18
hs	Slot depth	13.4, mm
d_{so}	Slot opening depth	1.6, mm
b_{so}	Slot opening length	2.4, mm
W_t	Teeth width	3.5, mm
D_{ext}	Stator outer diameter	123.8, mm
D	Air gap diameter	72, mm
L	Stack length	525, mm
D_{sh}	Shaft diameter	35, mm
N_s	Number of winding turns	12

It is observed that the effects of slot opening, armature reaction and saturation are not taken into account in the calculated waveforms. In the following, functions (1), (2) and (5) will be developed to include various effects in the calculated model.

2.1 | Inverse air gap function with slotting effect

In the first step of developing the analytical model, we attempt to include the slotting effect in the inverse air gap function of the SMPMSM. For this, Figure 2 is considered as the basis of the modeling. As shown in Figure 2, in the approximated form of the air gap distribution, we propose inverse air gap function distribution for a slot pitch as follows:

$$g_{so}^{-1}(\varphi_r)=\begin{cases}\left(\dfrac{0.5}{g_0+d_{s0}}+\dfrac{0.5}{g_0}\right)+\left(\dfrac{0.5}{g_0}-\dfrac{0.5}{g_0+d_{s0}}\right)\cos\left(\dfrac{2\pi}{D\tau_s}\varphi_r\right), & D\tau_s\geq\varphi_{\mathrm{r}}>0\\ \dfrac{1}{g_0}, & \tau_s\geq\varphi_{\mathrm{r}}>D\tau_s\end{cases} \tag{6}$$

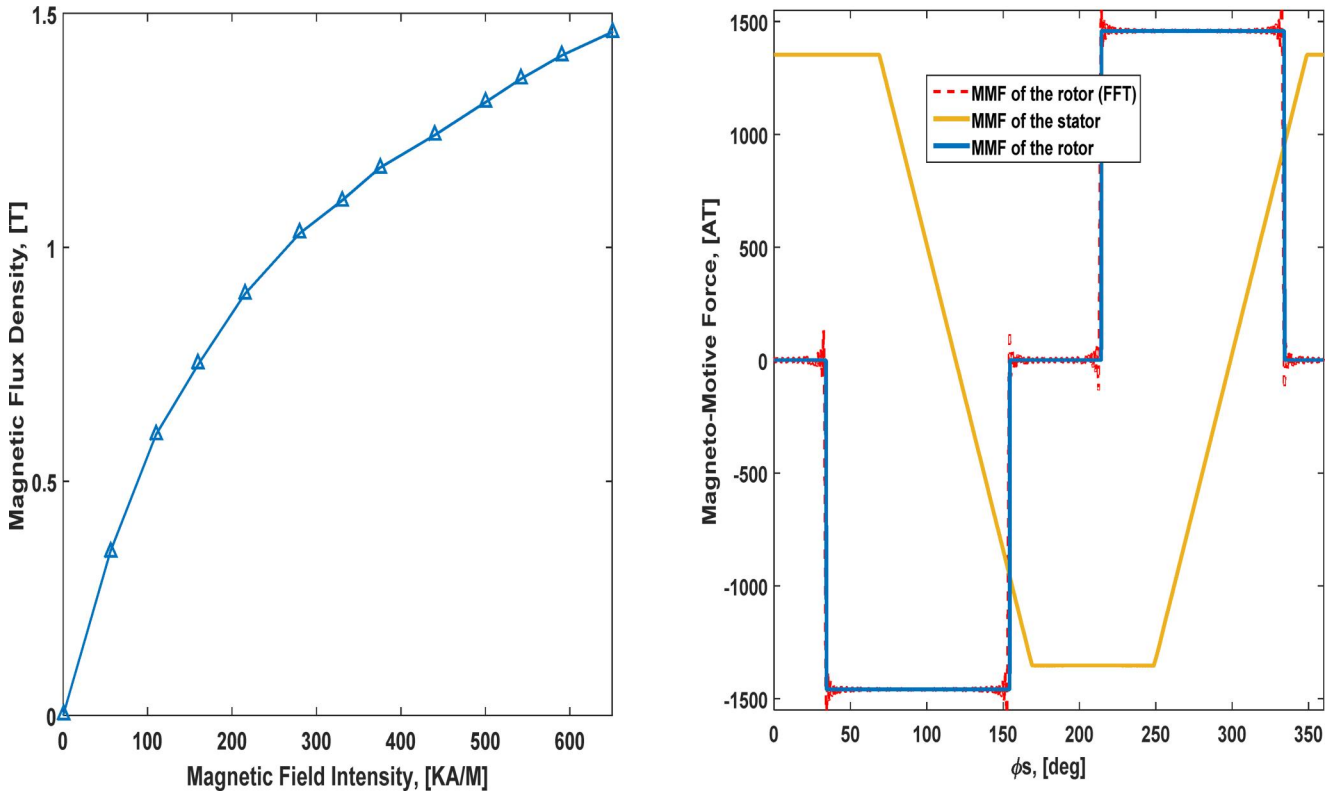

FIGURE 1 (Left): B-H curve of the steel-1008 lamination, (right): calculated winding MMF and rotor MMF distribution for the 2-poles SMPMSM at an arbitrary condition.

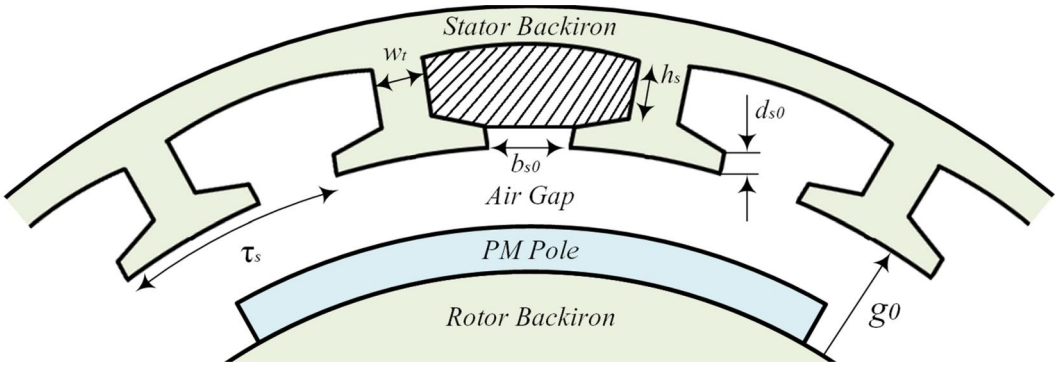

FIGURE 2 A part of a sample of the SMPMSM for modeling.

where τ_s is the slot pitch $\left(\frac{2\pi}{Q_s}\right)$ and D is the ratio of the slot opening angle to slot pitch $\left(\frac{b_{s0}}{\tau_s}\right)$. Also, the parameters d_{s0} and b_{s0} are denoted as the height of the teeth tip and slot opening, respectively. In this proposed relation, using the four defined variables, inverse air gap length has been predicted taking into account the sinusoidal variation of the slotting effect. For the 2-poles SMPMSM with $Q_s = 18$-*slots*, the Fourier series of the (6) are shown in Figure 3 for a quarter of the circumference. It is observed that with a real consideration of the slotting effect and with good accuracy, the length of the inverse air gap can be approximated. This characteristics can be adopt to the happened in the practical prototype SMPMSM. Also, the proposed function has been able to model the inverse air gap variation similar to the precise permeance function proposed in [33].

2.2 | Modeling of armatures reaction effect

A cross-sectional view of a two-pole surface-mounted PMSM for illustrating the development of the armature reaction (AR) model is proposed in Figure 4. In this case, the direction of the phasor is determined for arbitrary operation mode (lagging) and load condition. It can be observed that the armature current (I_a) lags behind the applied phase voltage (V_φ) by the

angle θ (power factor angle). The armature current creates stator magnetic field (B_s) and produces voltage (E_s) of its own in the stator. This armature reaction voltage coincides with the mmf phasor of the armature winding (F_{ar}). The F_{ar} can be resolved into the d-axis component, $F_{ar,d}$, and the q-axis component, $F_{ar,q}$, as illustrated in Figure 4. Also, the rotor magnetic field (B_r) produces an internal generated voltage (E_a) and the mmf phasor of the PM pole ($F_{d,pm}$) in the direction of the d-axis.

It is observed that the total MMF phasor of the d-axis ($F_{d,T}$) is obtained as follows:

$$F_{d,T} = F_{d,\mathrm{pm}} - F_{\mathrm{ar},d} \tag{7}$$

and the amplitude of the resultant MMF phasor at air gap (F_T) can be written as follows:

$$|F_T| = \left|F_{d,T} + F_{\mathrm{ar},q}\right| = \left|F_{d,\mathrm{pm}} - F_{\mathrm{ar},d} + F_{ar,q}\right| \tag{8}$$

Also, it is observed that the F_T angle lags δ degree ($F_T^{\angle -\delta}$) from the applied voltage. It can be concluded that the AR phenomenon in this mode operation of the motor could be change the amplitude and angle of the total MMF in the air gap. It is shown that the shift angle (δ) in this situation is the same with the power angle. Therefore, this angle dependent to the load torque can be calculated as follows:

$$\delta(T_L) = \tan^{-1}\left(\frac{|F_{\mathrm{ar},q}|}{|F_{d,T}|}\right) = \sin^{-1}\left(\frac{T_L \omega_m X}{3V_\varphi E_a}\right) \tag{9}$$

where the T_L and X are the load torque and self-inductance of armature reaction, respectively. Due to the constant rotor

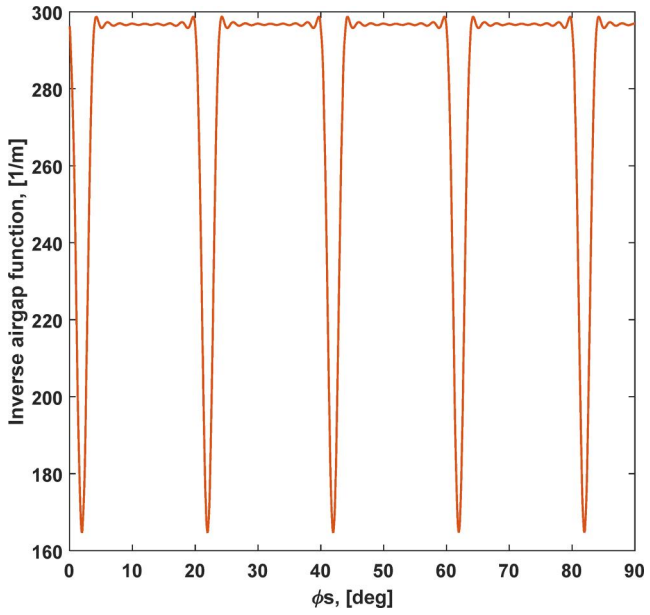

FIGURE 3 Inverse air gap function of the SMPMSM with the slot opening effect.

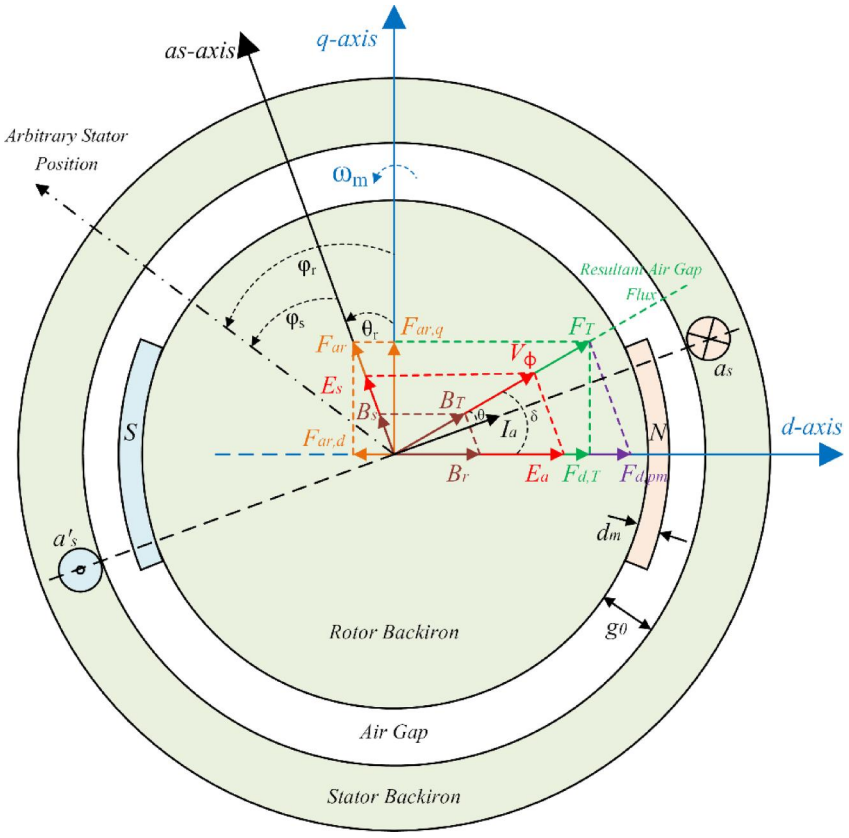

FIGURE 4 Proposed phasor diagram of the SMPMSM for AR modeling.

magnetic flux, the amplitude of the E_a in all steady state conditions is constant. Therefore, the change of the load torque in the SMPMSM can lead to changes in δ and the armature current in terms of amplitude (I_a) and power factor angle (θ), according to the following equation:

$$I_a(\delta(T_L),\theta(T_L)) = \frac{V_{\varphi}^{\angle 0} - E_a^{\angle -\delta}}{jX} = |I_a(\delta(T_L),\theta(T_L))|^{\angle \theta} \quad (10)$$

In the above equation, the value of R_A (phase resistance) has been neglected due to its smallness. The above relationship directly affects the magnitude and direction of the armature MMF (F_{ar} as shown in Figure 4), and this effect is modeled in the armature MMF distribution function as follows:

$$\text{MMF}_{s\_\text{AR}}(\varphi_s,\theta_r,T_L) = \sum_{n=1}\frac{3}{2}\frac{2}{\pi}\frac{N_s K_w}{n} I_a(\delta(T_L),\theta(T_L),T_L) \cos(\theta_r - nP\varphi_s - \varnothing_i - \theta) \quad (11)$$

It is important to mention that the value δ (or the load angle) does not directly affect the function MMF_{s_AR} of Equation (11) as it is wrongly stated in Equation (2) at [33]. Figure 4 shows if the voltage applied to the motor is considered with zero phase $\left(V_{\varphi}^{\angle 0}\right)$, the angle of $\text{MMF}_{\text{pm\_AR}}$ (or angle of $F_{d,T}$ or E_a) affected directly by load torque ($\delta(T_L)$) and proposed in constant amplitude for 2-poles SMPMSM as follows:

$$\text{MMF}_{\text{pm\_AR}}(\varphi_r,\delta(T_L)) = \begin{cases} -\dfrac{d_m B_m}{\mu_0(1+\chi)}, & \alpha_0+\delta+\alpha_{\text{pm}} \geq \varphi_{\text{r}} > \alpha_0+\delta \\ 0, & \alpha_0+\delta+\pi \geq \varphi_{\text{r}} > \alpha_0+\delta+\alpha_{\text{pm}} \\ \dfrac{d_m B_m}{\mu_0(1+\chi)}, & \alpha_0+\delta+\alpha_{\text{pm}}+\pi \geq \varphi_{\text{r}} > \pi+\alpha_0+\delta \end{cases} \quad (12)$$

In [33] (at Equation (3)), this $\text{MMF}_{\text{pm\_AR}}$ function is given wrongly without including δ. In the following, the variation of the armature reaction effect caused by T_L changes, which are aggregated through I_a, θ and δ in $\text{MMF}_{\text{s\_AR}}$ and $\text{MMF}_{\text{pm\_AR}}$ functions, is modeled as a resulting MMF of the air gap as follows:

$$\text{MMF}_{R\_\text{AR}}(\varphi_s,\theta_r,T_L) = \text{MMF}_{s\_\text{AR}}(\varphi_s,\theta_r,T_L) + \text{MMF}_{\text{pm\_AR}}(\varphi_r,\delta(T_L)) \quad (13)$$

Finally, considering the variation in the air gap length caused by the effect of slot opening (in relation (6)), the flux density distribution in the air gap of the SMPMSM can be calculated taking into account the effects of armature reaction and slot opening as follows:

$$B_{so\_\text{AR}}(\varphi_s,\theta_r,T_L) = \mu_0 \text{MMF}_{R\_\text{AR}}(\varphi_s,\theta_r,T_L) g_{so}^{-1}(\varphi_r) \quad (14)$$

In the next sub-section, we take into account the effect of magnetic saturation, in connection with Equation (13), in the model.

2.3 | Modeling of the saturation effect

In order to include the magnetic saturation effect in the AGFD model of the SMPMSM precisely, special attention should be paid to the connection of this phenomenon with the armature reaction effect. It seems that this dependence has not been considered in the literatures so far [34–36]. As shown in the above mathematical relations and Figure 4, in the resulting waveform of the MMF of the air gap, the change in value of the T_L influenced the I_a, θ and δ. Therefore, the distortion created in $\text{MMF}_{\text{R\_AR}}$ waveform can be the source of the magnetic saturation, especially in the teeth of the armature core, which is located above and near the PM poles. In this section, an effort is made to put the resulting distortion in connection with the magnetization curve of the stator core. In real conditions, it can be said that when the resultant MMF of the air gap ($|\text{MMF}_{\text{R\_AR}}|$) passes through the MMF of the knee point (MMF_{kp}) of the magnetization curve, the magnetic saturation will occur in the teeth that are located near or above the poles of the permanent magnet. It depends on how the distorted MMF_{R_AR} waveform is distributed at air gap. The magnetic saturation may also occur in the stator yoke or rotor core, but this possibility is usually more and more severe in teeth. This phenomenon leads to a limited and low increase in air gap flux density compared to the linear condition.

As shown in the previous section, with changes in load torque (T_L), the variables such as I_a, θ and δ are changed nonlinearity. Also, these three variables were incorporated into the MMF_{R_AR} function model in relation (13), which were able to model the effect of the armature reaction effectively. Therefore, by having the values of relative permeability of the magnetic laminations ($\mu_{r,\text{ sat}}$) at each point of the MMF_{R_AR} waveform, it can be written for the resultant air gap flux density ($B_{so\_\text{AR\_sat}}$) affected by both armature reaction and magnetic saturation as follows:

$$B_{so\_\text{AR\_sat}}(\varphi_s,\theta_r,T_L,\mu_{r,\text{sat}}) = \mu_0 \text{MMF}_{R\_\text{AR}}(\varphi_s,\theta_r,T_L) g_{so}^{-1}(\varphi_r) - \Delta B(\varphi_s,\theta_r,T_L,\mu_{r,\text{sat}}) \quad (15)$$

in which the ΔB is the saturation function that models the amount of decrease in air gap flux density according to the MMF_{R_AR} and the data of the core magnetisation curve ($\mu_{r,\text{ sat}}$, MMF_{kp}) as proposed below:

$$\Delta B = \begin{cases} 0, if\ |\mathrm{MMF}_{R\_\mathrm{AR}}| < \mathrm{MMF}_{kp} \text{ and } g_{so}^{-1}(\varphi_r) < \dfrac{1}{g_0} - \Delta g\_\mathrm{inv} \\ \mu_{r,\mathrm{sat}(\mathrm{MMF}_{R\_\mathrm{AR}})}\mu_0\left(\mathrm{MMF}_{R\_\mathrm{AR}} - \mathrm{MMF}_{kp}\right)g_{so}^{-1}(\varphi_r), \\ if\ |\mathrm{MMF}_{R\_\mathrm{AR}}| > \mathrm{MMF}_{kp} \text{ and } \dfrac{1}{g_0} \geq g_{so}^{-1}(\varphi_r) \geq \dfrac{1}{g_0} - \Delta g\_\mathrm{inv} \end{cases} \quad (16)$$

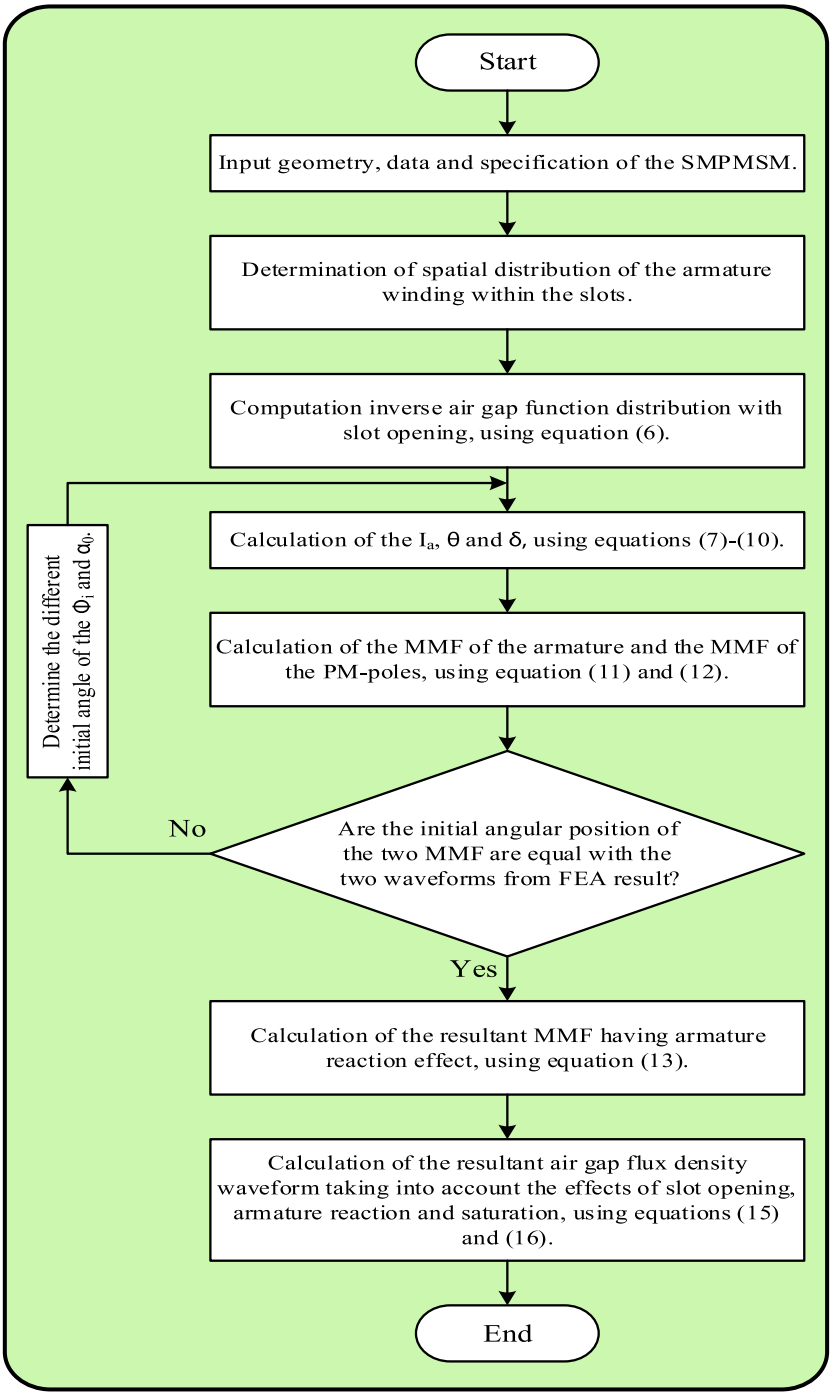

FIGURE 5 The flowchart of the proposed method.

The flowchart that describes the step-by-step implementation of the proposed method is shown in Figure 5 for better clarification.

The recent Equations (15) and (16) are based on the fact that the saturation may be occurred in the teeth (due to the small length of the air gap) or the slight angular positions (Δg_inv) between themes, where the value of the MMF_{R_AR} is greater than the value of the MMF_{kp} and a tooth (or a percent of teeth-pitch dependent to the Δg_inv) is located in that position. As can be seen, the proposed Equation (16) is a non-linear with a high coupling function based on (1) the value of the load torque connected, (2) MMF_{R_AR} waveform distribution, (3) the data of magnetisation characteristics of lamination material, and (4) the air gap length variation between the PM poles and teeth capable of taking into account the effects of saturation, armature reaction and slot opening (entirely and as a function of each other) for the AGFD waveform prediction of the SMPMSM. In the following, analytical simulation and finite element analysis (FEA) are implemented to analyse the sensitivity and estimate the accuracy of the proposed method.

3 | SIMULATION RESULTS

In order to simulate the proposed model and sensitivity analysis, the rated value and the nameplate data of the SMPMSM are given in Table 2. Based on these data and using the above-mentioned equations, the values of the useful variables, such as armature current, angle of power factor and the torque angle, are calculated due to the load torque variation in a steady state. The calculated data are gathered in Table 3. It is observed that when the value of the load torque is increased, the working condition of the SMPMSM changes from leading to lagging mode. Also, the amplitude of the I_a and δ is increased non-linearly. The three calculated variables are used in self-situation at the above-mentioned non-linear equations to simulate the AGFD of the SMPMSM assuming the 50% and 100% of the load torque is connected. The simulated results for the two cases are shown in Figure 6. It is observed and concluded that (1) the AGFD of the PM poles has the same variation in both conditions except that an angular shift of −33.12° has occurred, (2) the AGFD of the stator windings in a full-load condition has suffered more distortion compared to the 50% of the rated load torque condition due to the increasing of the I_a and θ, (3) more disturbances have occurred at the resultant AGFD in the rated condition due to the non-linear effect of the increasing of the I_a, δ and θ, and (4) the saturation phenomenon is arisen at the tip teeth above the PM poles and it includes a larger surface of the teeth in 50% of the rated load conditions.

TABLE 2 Rated value and nameplate data of the SMPMSM.

Specification	Values
Output power	97, kw
Frequency	50, Hz
Armature phase voltage	1354, V
Armature phase current	33.2, A
Power factor	0.9, lagging
Efficiency	0.8
No. of PM poles	2

3.1 | FE analysis results

In order to estimate the accuracy of the results of the proposed model, the exact method of FE is implemented in this section using Ansys Maxwell V16 FE package. For this, the SMPMSM with geometry and specifications given in Tables 1 and 2 is considered. To calculate the AGFD waveform of the SMPMSM using FE analysis, (a) a contour is drown at the middle of the air gap, (b) the amplitude of the AGFD is calculated on this contour for different rotor positions from 0° to 360° taking 0.1° steps, and (c) the same conditions for load torque variation (as illustrated in Table 3) are implemented. Figure 7 reveals the FE results of the flux density distribution in the SMPMSM cross-section at the arbitrary rotor position in the case of full-load and 50% conditions. It indicates that the saturation could occur at the corner of the tip teeth at 50% of the load torque. In accordance with what was described above, the saturation effects is occurred at some teeth in 50% of the load torque condition. Also, at full-load conditions, this effect is not observed at all.

Figure 8 shows a cycle (360°) of the AGFD waveform of the SMPMSM assuming the 50% and 100% of the load torque compared to the analytic proposed model results. From this figure, the following items can be taken and extracted:

(1) In 50% of the full-load condition, the SMPMSM will be placed in the lagging region and with the further increase in the I_a and δ; further shift and distorting may be

TABLE 3 Variation of the variables at a steady state used in the modeling of armature reaction effect of the SMPMSM.

Description	Symbols	Values				
Percent of rated load	$\%T_L$	No-load	25%	50%	75%	100%
Armature current	I_a	3.5, A	7.56, A	14.9, A	23.1, A	33.2, A
Angle of power factor	Θ	+32.68°	+9.43°	−4.94°	−15°	−26°
Torque Angle	δ	−4.88°	−12.2°	−25.18°	−39.6°	−58.3°
Internal generated voltage	E_a	1437.6,V	1437.6, V	1437.6, V	1437.6, V	1437.6, V

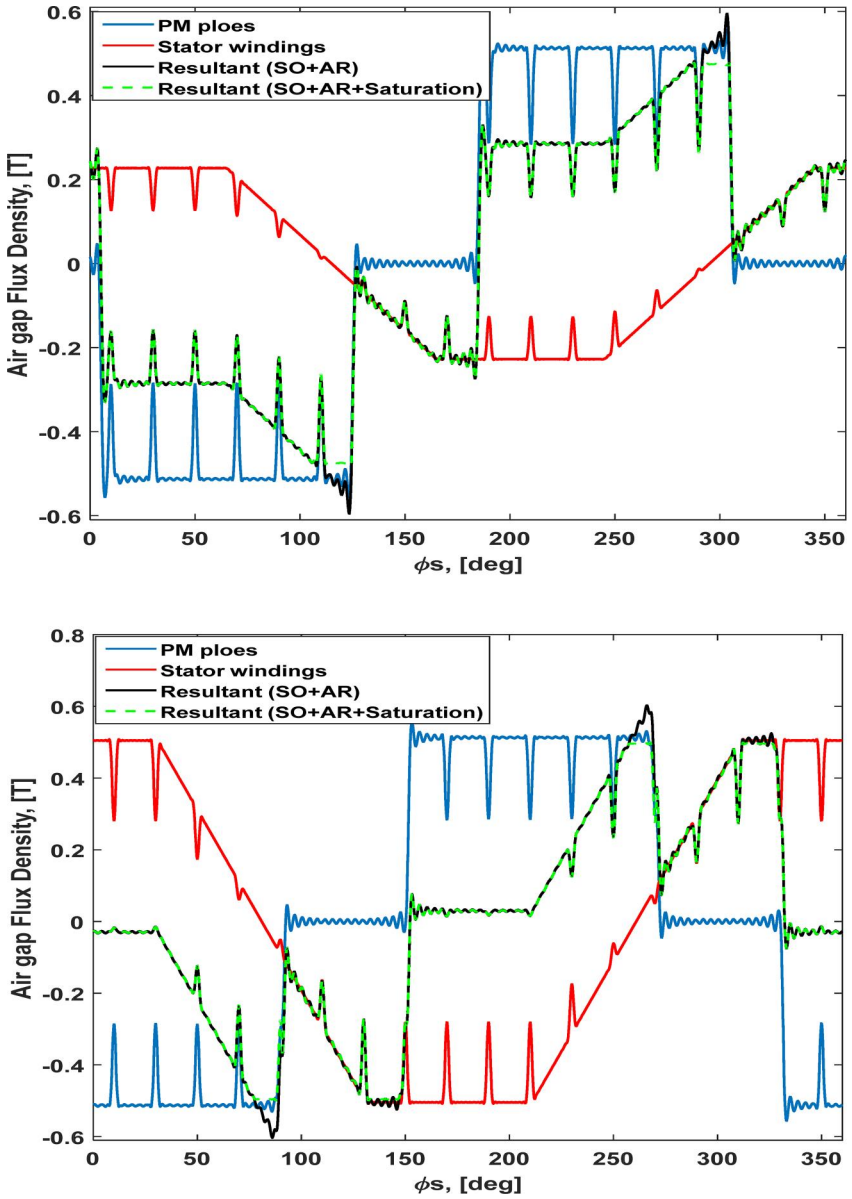

FIGURE 6 Simulation of the AGFD of the SMPMSM at (top): 50% and (bottom): full load.

occurred at the AGFD waveform. Also, the distorted resultant MMF at the air gap may cause saturation at some teeth (as it happened here).

(2) In a condition where 100% of the load torque is connected, the value of the I_a and δ increased more and more and the SMPMSM sinks deeper into the lagging region (adopt with results from Table 3). This event leads to a lot of reduction and distortion at the AGFD waveform compared to the mode of 50%. As can be seen, the phenomenon of magnetic saturation did not occur in these cases. This is the truth that actually happens and the saturation effect is completely dependent on the armature reaction effect. In addition, these two effects, in turn, have a non-linear dependence on load connection conditions, as shown in the model, proposed relationships, and analysis results.

(3) According to the modeling done, the severity of armature reaction and the magnetic saturation phenomena in the SMPMSM is completely non-linear and unpredictable and can only be calculated through the non-linear model and considering the motor's operating conditions and specifications.

(4) This proposed model capable of taking into account the effects of saturation, armature reaction and slot opening entirely and as a function of each other. Therefore, a small deviation in the prediction of input variables and waveforms of the proposed model affects the accuracy of the proposed model results compared to the FEA results. As can be seen in Figure 8 (top), good agreement between the analytic and FEA results is achieved at 50% full load, while in Figure 8 (bottom), the tracking of the results is good, but low accuracy in amplitude prediction has been occurred at full load

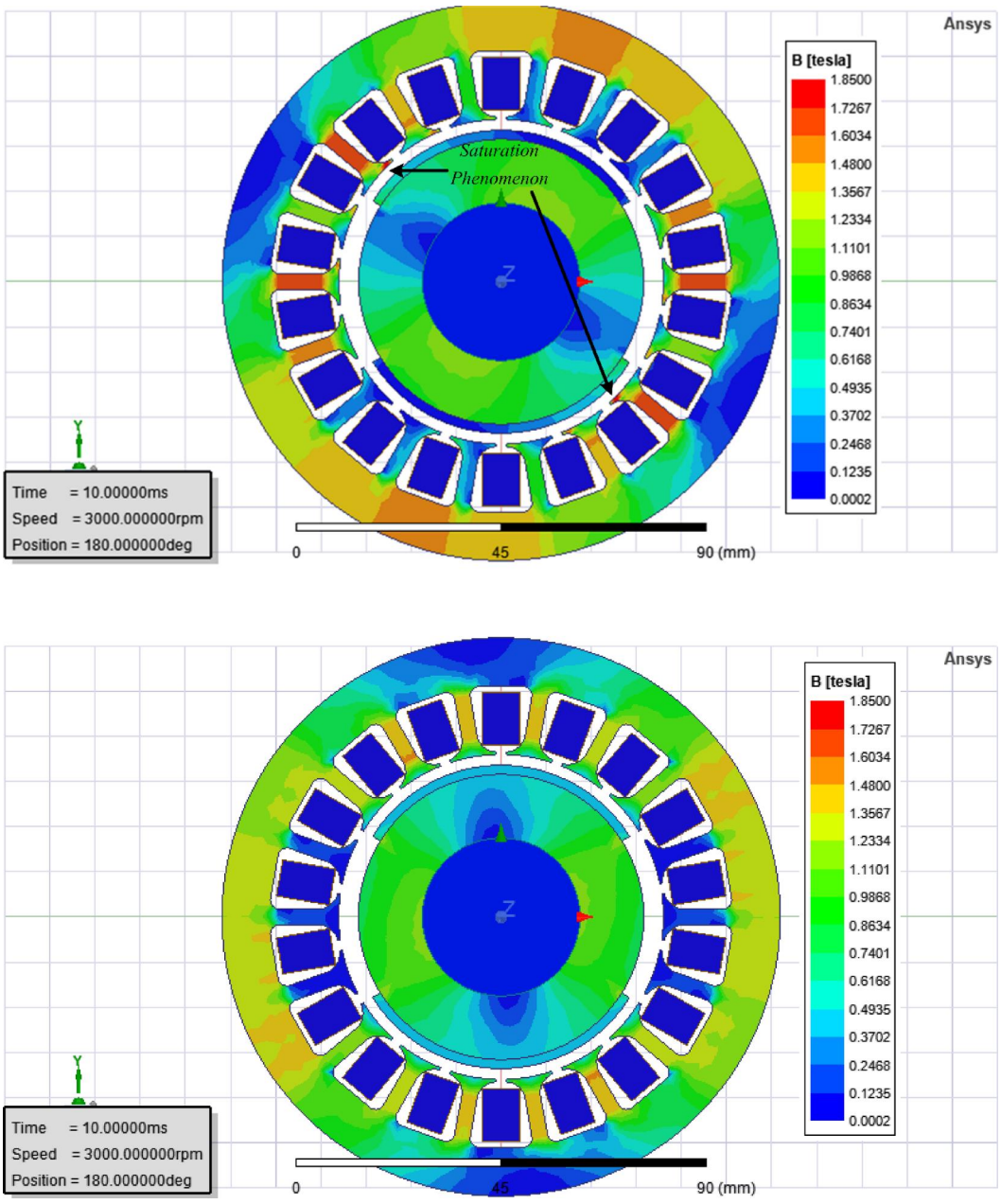

FIGURE 7 Flux density distribution in the SMPMSM at arbitrary rotor position, (top): 50%, and (bottom):100% of the full load.

due to the mentioned reasons. Therefore, the results of these figures and the proposed relations fully confirm the described non-linear modeling method.

4 | CONCLUSION

In this work, a comprehensive approach to model the AGFD waveform of the SMPMSM was presented. This model is capable of predicting the AGFD waveform at different operation conditions due to the load torque variation. Based on the proposed approach, a new form of AGFD was proposed, in which the following aspects are caused due to improved precision and applicability compared to the available approaches:

(1) The real form of the inverse air-gap distribution (slot opening) and spatial distribution of the MMF of the stator and PM poles are considered.
(2) The armature reaction effect related to the load torque variation is incorporated at the MMF distribution models of the armature and PM poles analytically.
(3) The effects of the magnetic saturation modeled as a new non-linear analytical function are dependent on the load torque and the data of magnetization characteristic of the lamination material.

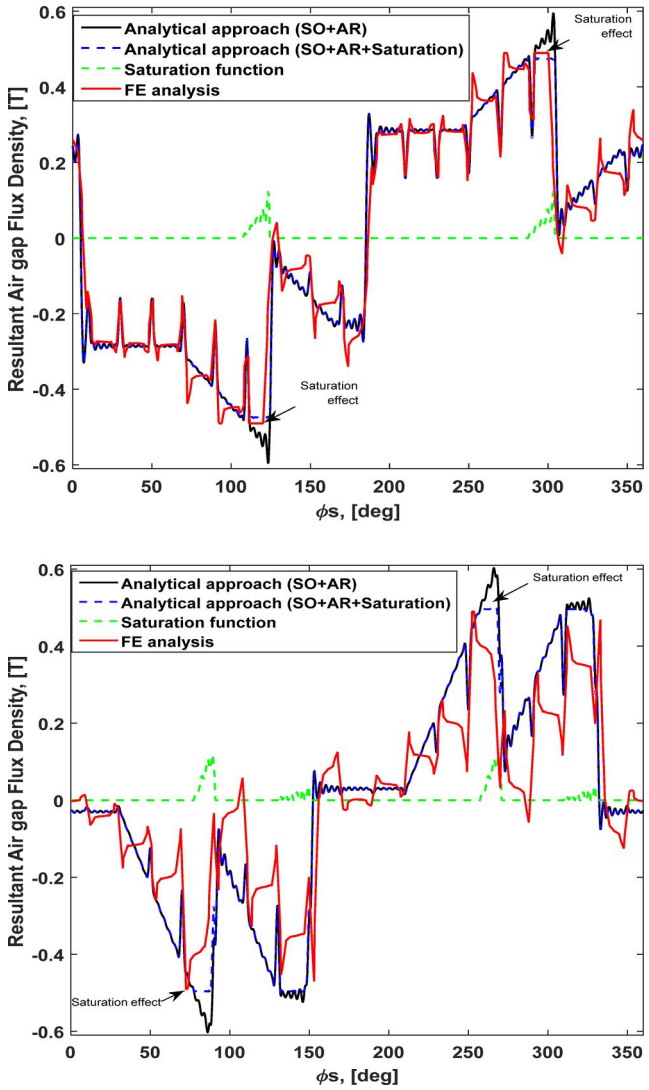

FIGURE 8 The results of the AGFD waveform prediction using the analytical proposed model and FE analysis, (top): 50% of full-load, (bottom): full-load condition.

(4) The proposed model is capable of taking into account the effects of slot opening, armature reaction and saturation phenomenon entirely and dependent on each other with coupling.

The proposed approach results were calculated by the simulation. In addition, FE analysis is implemented to evaluate the accuracy of the new model. It is shown that the proposed model results used to predict the AGFD waveform of the SMPMSM have a good agreement with the FE analysis results.

The authors will be intended to extend the proposed model for the inductance calculation and performance dynamic prediction of the SMPMSM in healthy and faulty conditions.

AUTHOR CONTRIBUTIONS

Mojtaba Babaei: Conceptualization; Formal analysis; Investigation; Supervision; Writing – original draft. **Mojtaba Feyzi**: Conceptualization; Formal analysis; Investigation; Supervision; Writing – original draft. **Abbas Nazari Marashi**: Funding acquisition; Resources; Writing – review and editing.

ACKNOWLEDGEMENTS

There is not any funding to report for this submission.

CONFLICT OF INTEREST STATEMENT

None of the authors have any conflicts of interest.

DATA AVAILABILITY STATEMENT

No data are available.

ORCID

Mojtaba Babaei https://orcid.org/0000-0003-4260-2133

REFERENCES

1. Misir, O., Raziee, S.M., Ponick, B.: Determination of the inductances of salient Pole synchronous machines based on the voltage equation of a single coil in the stator winding. IEEE Trans. Ind. Appl. 52(No.5), 3792–3804 (2016). https://doi.org/10.1109/tia.2016.2569065
2. Sun, H.Y., Wang, K.: Effect of third harmonic flux density on cogging torque in surface-mounted permanent magnet machines. IEEE Trans. Ind. Electron. 66(No.8), 6150–6158 (2018). https://doi.org/10.1109/tie.2018.2875639
3. Yamazaki, K., Utsunomiya, K., Ohiwa, H.: Mechanism of torque ripple generation by time and space harmonic magnetic fields in permanent magnet synchronous motors. IEEE Trans. Ind. Electron. 69(No.10), 9884–9894 (2022). https://doi.org/10.1109/tie.2021.3121713
4. Liu, C., et al.: Permanent magnet shape optimization method for PMSM air gap flux density harmonics reduction. CES Trans. Elect. Mach. Syst. 5(No.4), 9284–9290 (2021). https://doi.org/10.30941/cestems.2021.00033
5. Bahramgiri, M., et al.: A new structure of stator pole to reduce torque ripple and acoustic noise in switched reluctance motor. Proc. XVIIth Int. Conf. Elect. Mach. (2006)
6. Abolfathi, K., Babaei, M., Ahmarinejad, A.: Designing optimal passive filters for transformers under harmonic conditions. Energy Proc. 141, 411–417 (2017). https://doi.org/10.1016/j.egypro.2017.11.052
7. Babaei, M., Feyzi, M., Nazari Marashi, A.: Study of bifurcation and chaos in scalar drive systems of permanent magnet synchronous machines. International Trans. Elect. Energy Syst. 31(No.9), e13023 (2021). https://doi.org/10.1002/2050-7038.13023
8. Vahid Zamani Faradonbeh, A., et al.: 2-D analytical No-load electromagnetic model for slotted interior permanent magnet synchronous machines. IEEE Trans. Energy Convers. 36(No.4), 3118–3126 (2021). https://doi.org/10.1109/tec.2021.3064034
9. Zamani Faradonbeh, V., et al.: Analytical modeling of slotted, surface-mounted permanent magnet synchronous motors with different rotor frames and magnet shapes. IEEE Trans. Magn. 57(No.1), 1–13 (2021). https://doi.org/10.1109/tmag.2020.3032648
10. Babaei, M., Feyzi, M., Nazari Marashi, A.: Extended Poincaré model and non-linear analysis of permanent-magnet synchronous motor scalar drive system. IET Power Electron. 15(9), 855–864 (2022). https://doi.org/10.1049/pel2.12273
11. Boroujeni, S.T., Jalali, P., Bianchi, N.: Analytical modeling of No-load eccentric slotted surface-mounted PM machines: cogging torque and radial force. IEEE Trans. Magn. 53(No.12), 1–8 (2017). https://doi.org/10.1109/tmag.2017.2748501
12. Ko, Y.-Y., et al.: Analytical method for overhang effect of surface-mounted permanent-magnet motor using conformal mapping. IEEE Trans. Magn. 54(No.11), 3118–3126 (2018). https://doi.org/10.1109/tmag.2018.2841017
13. Jalali, P., Boroujeni, S.T., Bianchi, N.: Analytical modeling of slotless eccentric surface-mounted PM machines using a conformal

transformation. IEEE Trans. Energy Convers. 32(No.2), 658–666 (2016). https://doi.org/10.1109/tec.2016.2640450
14. Zhang, L.: An efficient modeling of air gap and nonlinear analysis of magnetic equivalent circuit for large turbogenerators under No-load condition. IEEE Trans. Magn. 58(No.2), 1–8 (2021). https://doi.org/10.1109/tmag.2021.3125141
15. Mollaeian, A., et al.: 3-D sub-domain analytical model to calculate magnetic flux density in induction machines with semiclosed slots under No-load condition. IEEE Trans. Magn. 53(No.6), 1–5 (2017). https://doi.org/10.1109/tmag.2017.2658543
16. Gao, L., et al.: An improved analytical model of magnetic field in surface-mounted permanent magnet synchronous motor with magnetic Pole cutting. IEEE Access 9, 142804–142814 (2021). https://doi.org/10.1109/access.2021.3120205
17. Ma, C., et al.: Analytical model of open-circuit air-gap field distribution in interior permanent magnet machines based on magnetic equivalent circuit method and boundary conditions of macroscopic equations. IEEE Trans. Magn. 57(No.3), 1–9 (2021). https://doi.org/10.1109/tmag.2021.3051498
18. Yin, H., et al.: Improved open-circuit airgap field model for FSCW-STPM machines considering PM-MMF fluctuation. IEEE Trans. Ind. Electron. 69(No.6), 5547–5556 (2022). https://doi.org/10.1109/tie.2021.3088371
19. Waheed, A., Ro, J.-S.: Analytical modeling for optimal rotor shape to design highly efficient line-start permanent magnet synchronous motor. IEEE Access 8, 145672–145686 (2020). https://doi.org/10.1109/access.2020.3014718
20. Wu, L., et al.: A subdomain model for open-circuit field prediction in dual-stator consequent-Pole permanent magnet machines. IEEE Trans. Magn. 55(No.8), 1–12 (2019). https://doi.org/10.1109/tmag.2019.2909721
21. Ebrahimi, B., et al.: Eccentricity Fault identification in round rotor synchronous motors considering load variation. Przeglad Elektrotechniczny 87, 288–292 (2011)
22. Hanic, A., et al.: On-load analysis of saturated surface permanent magnet machines using conformal mapping and magnetic equivalent circuits. IEEE Trans. Energy Convers. 33(No.3), 915–924 (2018). https://doi.org/10.1109/tec.2017.2789322
23. Farshadnia, M., et al.: Analytical modeling of armature reaction air-gap flux density considering the non-homogeneously saturated rotor in a fractional-slot concentrated-wound IPM machine. IEEE Trans. Magn. 53(No.2), 1–12 (2017). https://doi.org/10.1109/tmag.2016.2623797
24. Ren, J., Wang, X., Zhao, W.: Magnetic field prediction of the saturated surface-mounted permanent magnet synchronous machine with rotor eccentricity. IEEE Trans. Ind. Electron. 69(No.8), 7756–7766 (2021). https://doi.org/10.1109/tie.2021.3105985
25. Oh, S., Min, S., Hong, J.-P.: Air gap flux density waveform design of surface-mounted permanent magnet motor considering magnet shape and magnetization direction. IEEE Trans. Magn. 49(No.5), 2393–2396 (2013). https://doi.org/10.1109/tmag.2013.2246142
26. Teymoori, S., et al.: 2-D analytical magnetic field prediction for consequent-Pole permanent magnet synchronous machines. IEEE Trans. Magn. 52(No.6), 1–14 (2016). https://doi.org/10.1109/tmag.2016.2521834
27. Li, J., Wang, K.: Analytical determination of optimal PM-Arc ratio of consequent-Pole permanent magnet machines. IEEE ASME Trans. Mechatron. 23(No.5), 2168–2177 (2018). https://doi.org/10.1109/tmech.2018.2865517
28. Zhu, M., et al.: Subdomain model for predicting armature reaction field of dual-stator consequent-pole PM machines accounting for tooth-tips. CES Trans. Elect. Mach. Syst. 3(No.2), 143–150 (2019). https://doi.org/10.30941/cestems.2019.00020
29. Zhuang, H., et al.: Magnetic analysis of skew effect in surface-mounted permanent magnet machines with skewed slots. IEEE Trans. Magn. 58(No.12), 1–12 (2022). https://doi.org/10.1109/tmag.2022.3208696
30. Krause, P., et al.: Analysis of Electric Machinery and Drive Systems, ed. IEEE Press (2013)
31. Polinder, H., Hoeijmakers, M.J., Scuotto, M.: Eddy-current losses in the solid back-iron of PM machines for different concentrated fractional pitch windings. IEEE Int. Elect. Mach. Drives Conf. (IEMDC) (2007)
32. Ishak, D., Zhu, Z.Q., Howe, D.: Comparison of PM brushless motors, having either all teeth or alternate teeth wound. IEEE Trans. Energy Convers. 21(No. 1), 95–103 (2006). https://doi.org/10.1109/tec.2005.853765
33. Dajaku, G., Gerling, D.: Stator slotting effect on the magnetic field distribution of salient Pole synchronous permanent-magnet machines. IEEE Trans. Magn. 46(No.9), 3676–3683 (2010). https://doi.org/10.1109/tmag.2010.2049269
34. Li, Z., et al.: Nonlinear analytical model for predicting magnet loss in surface-mounted permanent-magnet motors. IEEE Trans. Magn. 58(No.8), 1–5 (2022). https://doi.org/10.1109/tmag.2022.3156790
35. Song, Z., et al.: Field prediction and validation of a slotless segmented-halbach permanent magnet synchronous machine for more electric aircraft. IEEE Trans. Transport. Electrif. 6(No.4), 1577–1591 (2020). https://doi.org/10.1109/tte.2020.2982733
36. Yang, J., et al.: Accurate calculation of magnetic field of same-Pole and same-slot surface-mounted three-phase permanent magnet synchronous motor. IEEE Trans. Magn. 58(No.8), 1–10 (2022). https://doi.org/10.1109/tmag.2022.3183325

How to cite this article: Babaei, M., Feyzi, M., Nazari Marashi, A.: Incorporating the coupled effects of slot opening, armature reaction and saturation in the model of the airgap flux density distribution of permanent magnet synchronous machines. IET Electr. Power Appl. 18(2), 240–251 (2024). https://doi.org/10.1049/elp2.12384